DESIGN CONCEPTS FOR DAMAGE-FREE SEISMIC-RESISTANT SELF-CENTERING STEEL CONCENTRICALLY-BRACED FRAMES

D. Roke[1], R. Sause[2], J.M. Ricles[3], and N. Gonner[1]

[1] *Graduate Research Assistant, ATLSS Center, Department of Civil and Environmental Engineering, Lehigh University, USA*
[2] *Joseph T. Stuart Professor of Structural Engineering, ATLSS Center, Department of Civil and Environmental Engineering, Lehigh University, USA*
[2] *Bruce G. Johnston Professor of Structural Engineering, ATLSS Center, Department of Civil and Environmental Engineering, Lehigh University, USA*
Email: dar305@lehigh.edu, rsause@lehigh.edu, jmr5@lehigh.edu, npg207@lehigh.edu

ABSTRACT :

Self-centering concentrically-braced frame (SC-CBF) systems are being developed with the goal of providing adequate nonlinear drift capacity without significant damage or residual drift under the design basis earthquake. Analytical pushover and dynamic analyses were performed on several SC-CBF configurations to evaluate their response to earthquake loading. Each SC-CBF self-centered under earthquake loading. Some loss of post-tensioning occurred in one configuration. The dynamic response of the SC-CBF systems, however, was consistent with the intended behavior.

A procedure is presented herein to calculate the design demands for the frame members. This design procedure is then validated with analytical results. Analysis results show that the design procedure accurately predicts the member force demands under earthquake loading.

KEYWORDS: Post-tensioned steel braced frame, self-centering

1. INTRODUCTION

Steel concentrically-braced frame (CBF) systems are stiff and economical earthquake-resistant steel frame systems, which often exhibit limited system ductility capacity. The ductility capacity can be increased through the use of buckling-restrained braces (e.g., Fahnestock et al. 2003); however, the buckling-restrained braced frame system sometimes exhibits significant residual drift after an earthquake. To increase the ductility and reduce the residual drift of CBFs, self-centering concentrically-braced frame (SC-CBF) systems are being developed.

Recent research on self-centering (SC) unbonded post-tensioned (PT) precast wall systems (e.g., Kurama et al. 2002), on frames with inclined and vertically oriented draped PT tendon systems (Pekcan et al. 2000), and on SC steel moment-resisting frames with PT connections (e.g., Ricles et al. 2001, 2002; Garlock et al. 2005; Rojas et al. 2005) suggests that self-centering system concepts can be applied to CBFs. As part of a larger project on self-centering steel frame systems, ongoing research at Lehigh University is developing concepts, details, and design criteria for SC-CBF systems.

2. SYSTEM BEHAVIOR

The SC-CBF system and its idealized behavior are shown schematically in Fig. 1. The system consists of beams, columns, and braces in a conventional arrangement (Fig. 1(a)), with column base details that permit the columns to uplift at the foundation (Fig. 1(c)). Gravity loads and post-tensioning (PT) forces (from PT steel arranged along the column lines in the system shown in Fig. 1(a)) resist column uplift and provide a

restoring force after uplift. The beams, columns, and braces are intended to remain essentially elastic under the design earthquake, and the column uplift provides a mechanism for controlling the force levels that develop in the frame under earthquake loading.

Fig. 1(a) shows the loads used to simulate earthquake loading in pushover analyses of SC-CBFs. Design dead loads and live loads (*g*) are applied at the columns at each floor level. The lateral load profile (F_i) is based on an equivalent lateral force procedure (ICC 2003). Under low levels of lateral load, the structure deforms elastically as shown schematically in Fig. 1(b). This deformation is similar to that of a conventional CBF. Under higher levels of lateral load, the overturning moment at the base of the frame becomes large enough for the "tension" column to decompress, and uplift of the column occurs, as shown in Fig. 1(c). After column decompression and uplift, the lateral displacement of the frame is dominated by rigid body rotation of the frame about the base of the "compression" column, although some additional forces and deformations develop in the beams, columns, and braces of the frame. The PT steel elongates from the uplift of the frame, leading to an increase in PT force, which provides a positive stiffness after uplift to the lateral force-lateral drift behavior.
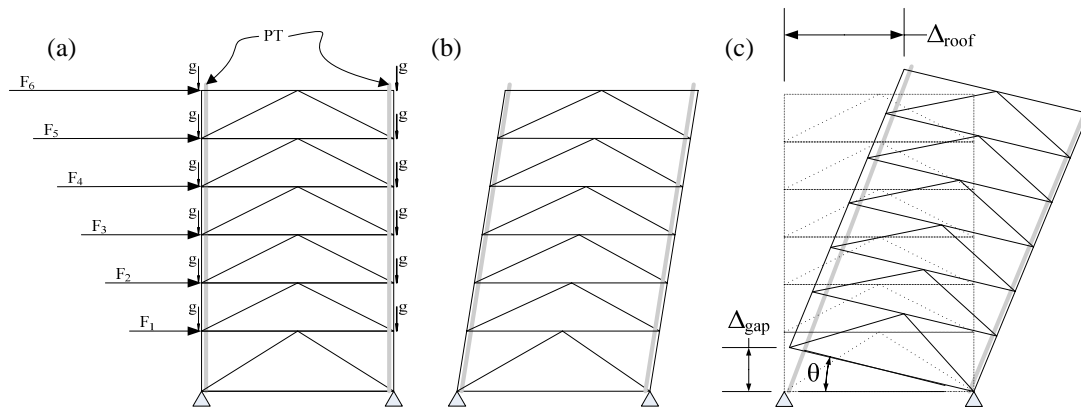
Figure 1. SC-CBF system: (a) schematic of members and loads; (b) elastic response prior to column decompression; (c) rigid-body rotation after column decompression.

3. FRAME CONFIGURATIONS

Three different SC-CBF configurations are considered in this study. Frame A is a typical braced-frame with PT steel added along each column line, as shown in Fig. 2(a). Frame A requires significantly stronger columns than a typical braced frame, because of the post-tensioning forces. Each member of the frame is designed to remain essentially elastic at force levels corresponding to PT yielding.

Frame D (Fig. 2(b)) consists of an SC-CBF placed between two additional columns that are attached to the gravity load system of the building. These two "gravity columns" alongside the SC-CBF separate the gravity load carrying function from the rocking of the SC-CBF. Energy dissipation (ED) elements are located between the gravity columns and the SC-CBF columns. The distribution of the ED elements throughout the height of the structure is intended to increase energy dissipation in the higher modes of vibration. The PT bars are located at midbay of the SC-CBF to reduce the elongation demand on the bars. As the gap opens at the column base, the elongation demand of the PT bars will be half of the gap-opening displacement of the uplifting column (Fig. 1(c)).

Frame D$_{DIST}$ (Fig. 2(c)) is a modification of Frame D, to which vertical "distribution" struts are added in the upper stories. These struts are intended to distribute the large PT forces to the braces over multiple stories, thereby reducing the concentration of force in the braces in the uppermost story.
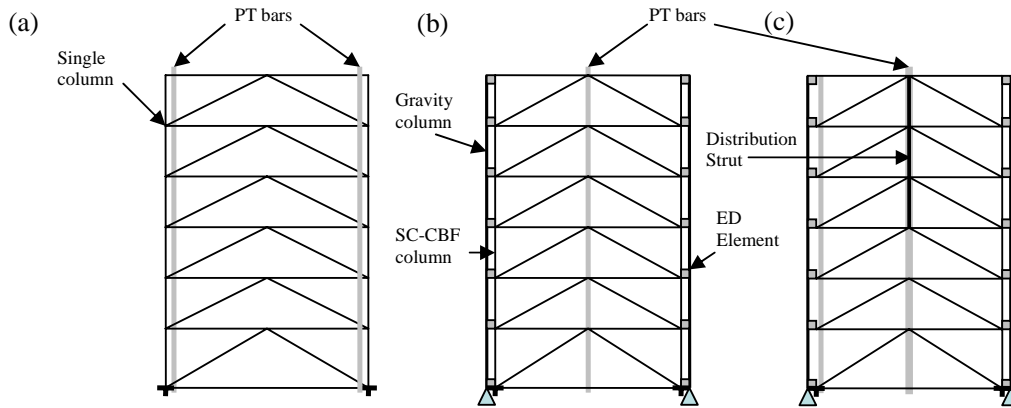
Figure 2.　Frame configurations:　(a) Frame A; (b) Frame D; (c) Frame D$_{DIST}$.

4. MEMBER FORCE DESIGN PROCEDURE

4.1. First Mode Forces

The calculation of member force design demands is critical for the SC-CBF system. The performance-based design criteria for the SC-CBF require the frame members to remain essentially elastic as the PT steel yields (Sause et al. 2006). Therefore, the SC-CBF member force design demands for the first mode correspond to the level of lateral load at which the PT steel yields.

To determine the first mode lateral forces, the modal mass distribution, $\{s_n\}$, is calculated using Equation (4.1):

$$\{s_n\} = \Gamma_n [m]\{\phi_n\} \tag{4.1}$$

where n is the mode number, Γ_n is the nth modal participation factor, $[m]$ is the mass matrix, and $\{\phi_n\}$ is the nth mode shape. For the first mode, $n = 1$. Multiplying this mass distribution by g, the acceleration due to gravity, produces the first mode force distribution. The first mode force distribution is scaled to produce yielding of the PT steel. To determine the scale factor, the ratio of the first mode overturning moment to the overturning moment causing PT yield is calculated using Equation (4.2):

$$\alpha_{1Y} = \frac{OM_Y}{OM_1} \tag{4.2}$$

where OM_1 is the first mode overturning moment (Equation (4.3)), and OM_Y is the overturning moment at which the PT bars yield, as determined from a free body diagram of the SC-CBF (Equation (4.4) for Frames D and D$_{DIST}$).

$$OM_1 = \{h\}^T \{s_1\}g \tag{4.3}$$

$$OM_Y = PT_y \frac{b_{SC-CBF}}{2} + V_{ED}\left(b_{SC-CBF} + 2s_{ED}\right) + W_{SC-CBF} \frac{b_{SC-CBF}}{2} \tag{4.4}$$

where $\{h\}$ is the vector of floor heights, b_{SC-CBF} is the center-to-center spacing of the SC-CBF columns, s_{ED}

is the spacing from the centerline of the SC-CBF columns to the line of action of the ED elements, PT_Y is the yield force capacity of the PT bars, V_{ED} is the sum of the force capacities of the ED elements on one side of the SC-CBF, and $W_{SC\text{-}CBF}$ is the weight of the SC-CBF.

To determine the member forces at PT yield, lateral forces equal to $\alpha_{1Y}\{s_1\}g$ are applied along with PT_Y, V_{ED}, and $W_{SC\text{-}CBF}$ to a linear elastic fixed-base model of the SC-CBF. The corresponding first mode member force demands are the moments and axial loads from this linear analysis.

4.2. Higher Mode Force Contribution

Nonlinear dynamic analyses under earthquake loading (Sause et al. 2006) have shown that the maximum member force demands during dynamic response exceed the first mode design demands. This result is illustrated in Figure 3, which shows the total and first mode overturning moment and base shear responses.

Figure 3(a) shows the total overturning moment and the first mode overturning moment responses from dynamic analysis, normalized by OM_Y. The first mode accounts for nearly all of the overturning moment response. Figure 3(b) shows the total base shear and the first mode base shear responses, normalized by the base shear at PT yield, V_{bY}, which is calculated according to Equation (4.5):

$$V_{bY} = \sum_{x=1}^{N} \alpha_{1Y} s_{1,x} g \tag{4.5}$$

where x is the floor level and N is the total number of floors. Note that in Figure 3(b), the higher modes are seen to contribute to the base shear response.
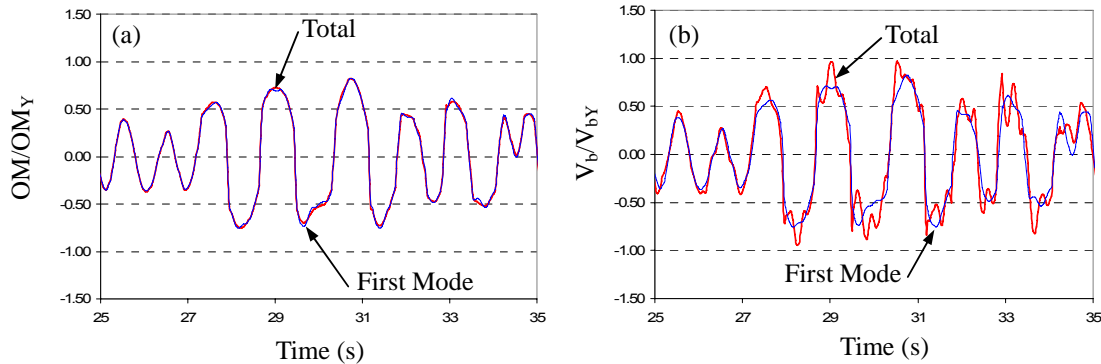
Figure 3.   Nonlinear analysis results: (a) overturning moment; (b) base shear.

The results in Figure 3(b) are similar to the member force demands throughout the structure. More accurate member force design demands must include higher mode response in addition to the first mode response. The higher mode responses can be determined by modal decomposition of the restoring force vector. For linear structural response to an earthquake ground motion, the restoring force vector in each mode, $\{f_{r,n}(t)\}$, can be expressed as the modal mass distribution, $\{s_n\}$, multiplied by the modal pseudo-acceleration, $A_n(t)$, whereby:

$$\{f_{r,n}(t)\} = \{s_n\}A_n(t) = \Gamma_n[m]\{\phi_n\}A_n(t) \tag{4.6}$$

$A_n(t)$ in Equation (4.6), however, is based on linear, not nonlinear, structural response. The rocking response of the SC-CBF system is nonlinear. Figure 4(a) shows the decomposition of the rocking displaced shape of the SC-CBF. The presence of higher modes in this rocking displaced shape is evident

in Figure 4(a). The rocking response increases the magnitude of the effective pseudo-acceleration in the nth mode, $\alpha_n(t)$, beyond the magnitude of the linear pseudo-acceleration $A_n(t)$. For the nonlinear response to a given earthquake ground motion, Equation (4.7) expresses the modal restoring force in terms of $\alpha_n(t)$.

$$\{f_{r,n}(t)\} = \{s_n\}\alpha_n(t) \tag{4.7}$$

$\alpha_n(t)$ is calculated from the nonlinear response as follows. First, the total restoring force vector, $\{f_r(t)\}$, is written as a summation of the modal restoring force vectors:

$$\{f_r(t)\} = \sum_{n=1}^{N}\{f_{r,n}(t)\} = \sum_{n=1}^{N}\Gamma_n[m]\{\phi_n\}\alpha_n(t) \tag{4.8}$$

Pre-multiplying each side of the equation by the nth mode shape gives the following result, due to the mass orthogonality of the mode shapes:

$$\{\phi_n\}^T\{f_r(t)\} = \Gamma_n\{\phi_n\}^T[m]\{\phi_n\}\alpha_n(t) \tag{4.9}$$

The effective modal pseudo-acceleration $\alpha_n(t)$ is then calculated from the total restoring force vector $\{f_r(t)\}$ as shown in Equation (4.10):

$$\alpha_n(t) = \frac{\{\phi_n\}^T\{f_r(t)\}}{\Gamma_n\{\phi_n\}^T[m]\{\phi_n\}} = \frac{\{\phi_n\}^T\{f_r(t)\}}{\Gamma_n M_n} \tag{4.10}$$
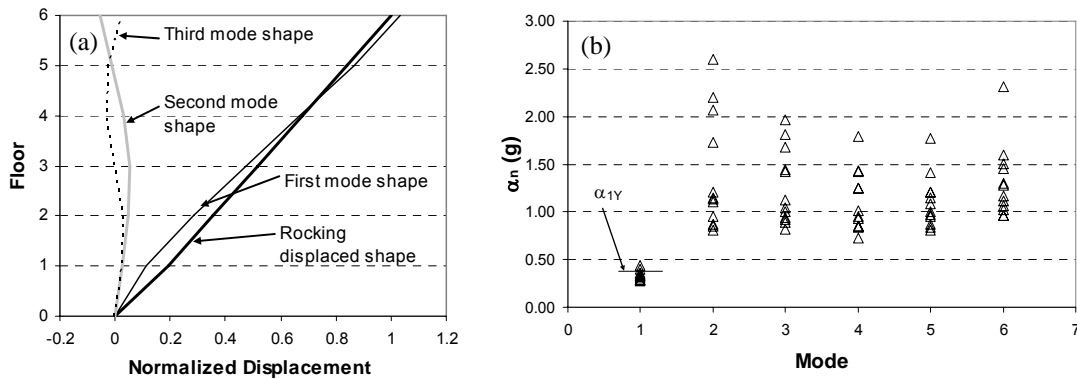
Figure 4. (a) Modal decomposition of rocking shape; (b) distribution of α_n from DBE-level seismic hazard.

For design purposes, the maximum value of $\alpha_n(t)$, denoted α_n, is of interest.

$$\alpha_n = \max|\alpha_n(t)| \tag{4.11}$$

Figure 4(b) shows the distribution of α_n values from a study of the DBE-level response of a six-story SC-CBF system. The value of α_1, the first mode effective pseudo-acceleration, has low dispersion and is close to α_{1Y}. The α_n values for higher modes reflect uncertainty in the degree to which the rocking behavior excites each mode.

For design purposes, it is preferable to use the spectral accelerations from a design spectrum for each mode, SA_n, rather than using α_n, where values of SA_n are determined from a smooth design response spectrum (e.g., BSSC 2003). To incorporate the uncertainty in the values of α_n, load factors γ_n are applied to SA_n for use

in design.   The values of γ_n were determined from probabilistic analysis of nonlinear response results for six-story SC-CBFs as follows:

$$
\begin{aligned}
p\left(\gamma_n \alpha_{1Y} < \alpha_n\right) &= 0.05 \qquad n = 1 \\
p\left(\gamma_n SA_n < \alpha_n\right) &= 0.05 \qquad n = 2 \ to \ N
\end{aligned}
\tag{4.12}
$$

From the probabilistic analysis of DBE-level response of six-story SC-CBF systems, the values of γ_n were selected as 1.15 for the first mode and 2.0 for the higher modes, based on Equation (4.12).

The modal member force design demands, r_n, are determined from a linear structural analysis of a fixed-base model of the structure subjected to the force vector $SA_n\{s_n\}g$ for the higher modes; the first mode force vector, $\alpha_{1Y}\{s_n\}g$, is applied with PT_Y and V_{ED} as described earlier.

Each modal member force demand, $r_{a,n}$ (where a designates the member and n is the mode), is then multiplied by the load factor γ_n for that mode.   To accommodate the significant correlation between the modal responses due to the rocking of the SC-CBF, the complete quadratic combination (CQC) method was used to determine the member force design demands.   The CQC equation is shown in Equation (4.11).

$$
r_{a,design} = \left(\sum_{i=1}^{N} \sum_{n=1}^{N} \rho_{in} \left(\gamma_i r_{a,i} \right) \left(\gamma_n r_{a,n} \right) \right)^{\frac{1}{2}}
\tag{4.11}
$$

where the coefficients of the correlation matrix $[\rho]$ are selected to approximate the correlation of the α_n values.   The diagonal values of $[\rho]$ are unity and the off-diagonal terms are tentatively set at 0.25, which is much larger than the usual $[\rho]$ coefficients for linear response.   Each frame member is then designed to resist the moment/axial load interaction of the corresponding design demands.

5. ANALYSIS RESULTS

To determine the dynamic response of the frame configurations discussed earlier, a suite of DBE-level ground motions was assembled.   The ground motions were scaled to the DBE level using the approach described by Seo and Sause (2005a).   Nonlinear time history analyses were then performed using OpenSEES.   The beams, columns, and braces of the frames were modeled as linear elastic so the member force demands required to keep the members linear elastic could be determined.   The PT steel was modeled using nonlinear truss-bar elements and the gap opening behavior was modeled using contact elements.   Rayleigh damping was used with a 5% damping ratio in the first and third modes.

The maximum roof drift response for each ground motion is shown in Figure 5(a).   The results are shown for each frame configuration discussed previously.   The member force design demands for Frames A, D, and D$_{DIST}$ were based on the first mode design demands only, with γ_1 equal to 1.0.   The member force design demands for Frame D$_{DIST}$v2 included the higher mode demands as well as the first mode demands, with γ_1 equal to 1.15, γ_2 through γ_6 equal to 2.0, and $[\rho]$ as described earlier.   The difference in roof drift for Frame D$_{DIST}$ and Frame D$_{DIST}$v2 is negligible, showing that the roof drift response is more a function of the frame configuration than the member design procedure.   Frames D, D$_{DIST}$, and D$_{DIST}$v2 all have lower roof drift demands than Frame A, largely due to the presence of the energy dissipation elements, which were not present in Frame A.

Figure 5(b) shows the maximum normalized brace force demand in each story from dynamic analysis for each ground motion.   Again, results are shown for each frame configuration.   The brace force demands are normalized by the design demand for each story.   A normalized brace force less than 1.0 represents a conservative design demand.   From these results, it can be seen that for Frames A, D, and D$_{DIST}$, the

member force demands from the dynamic response significantly exceed the member force design demands. This is due to the aforementioned higher mode response, which was not considered in the design demand calculations for these frames.   However, Frame $D_{DIST}v2$ was designed to account for higher mode demands as described above.   The results for Frame $D_{DIST}v2$ show that the demands from the dynamic analysis rarely exceed the design demands.
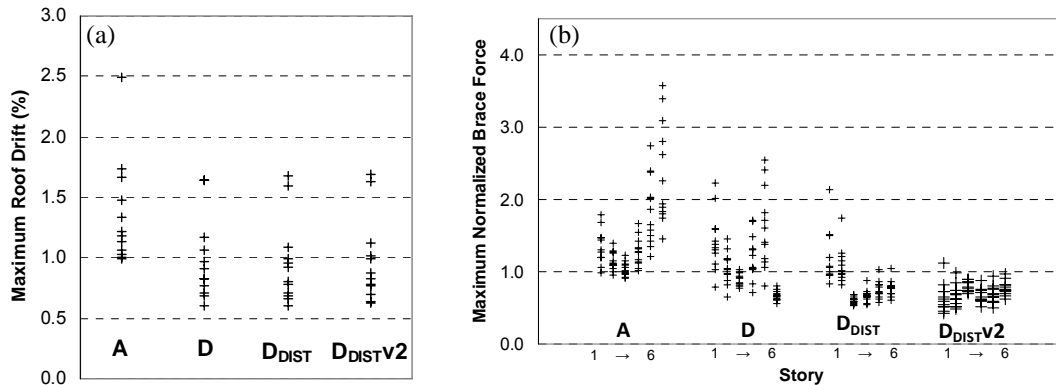
Figure 5.   Maximum dynamic analysis results for each frame configuration: (a) Roof drift; (b) Brace axial force, normalized by design demand.

Figure 5(b) shows the brace force demands for the sixth story of Frame D, where the PT steel is located at midbay, are also conservative.   This is due to the fact that the PT force contribution, which is included in the first mode design demand, dominates the brace force response in that story.   The mean normalized brace force for the sixth story is significantly lower than the mean value for the other stories; the dispersion is also significantly less.   The effect of the distribution strut is clearly visible in the results for Frame D_{DIST}, in which the domination of the PT force contribution to the brace force demand is extended to the uppermost 4 stories due to the distribution struts in stories 4, 5, and 6.

6. SUMMARY AND CONCLUSIONS

The paper describes the lateral force-lateral drift behavior of the SC-CBF system and three different frame configurations.   Seismic response analysis of these configurations show that the SC-CBF behaves as expected, and show the effect of different frame configurations on the dynamic response.   In addition, the results indicate that the addition of ED elements significantly reduces the dynamic drift demand on the SC-CBF and that the vertical distribution strut used in Frame D_{DIST} reduces the dispersion of brace force demand in the higher stories.

A probability-based design methodology was presented in this paper to determine member force design demands.   The dynamic analysis results show that these design demands safely account for the higher mode demands introduced by the nonlinear rocking response of the frame.

Ongoing work is studying the seismic response of SC-CBFs under a variety of seismic input levels, including both DBE and MCE levels, to more rigorously characterize the performance of SC-CBFs.   In addition, large-scale experiments are currently in development at the NEES RTMD facility at Lehigh University.

The results presented in this paper suggest that with further research, the overall goals of increasing the ductility and reducing the residual drift of concentrically braced frames can be reached, and that the specific SC-CBF performance objective of immediate occupancy performance under the DBE can be achieved.

REFERENCES

American Institute of Steel Construction (AISC), (2001). *Manual of Steel Construction – LRFD*, 3rd Edition.

Building Seismic Safety Council (BSSC), (2003). *NEHRP Recommended Provisions for Seismic Regulations for New Buildings and Other Structures, FEMA 450*, National Institute of Building Sciences, Washington, D.C.

Fahnestock, L.A., R. Sause, J.M. Ricles, and L.-W. Lu, (2003). "Ductility Demands on Buckling Restrained Braced Frames Under Earthquake Loading," *Journal of Earthquake Engineering and Engineering Vibration*, **2**(2), 255-268.

Garlock, M.M., J.M. Ricles, and R. Sause, (2005). "Experimental Studies on Full-Scale Post-Tensioned Steel Connections," *ASCE Journal of Structural Engineering*, **131**(3), 438-448.

International Code Council (ICC), (2003). *International Building Code*, ICC, Falls Church, VA.

Kurama, Y., R. Sause, S. Pessiki, and L.-W. Lu, (2002). "Seismic Response Evaluation of Unbonded Post-Tensioned Precast Walls," *ACI Structural Journal*, **99**(5), 641-651.

Pekcan, G., J.B. Mander, and S. Chen, (2000). "Experiment on Steel MRF Building with Supplemental Tendon System," *ASCE Journal of Structural Engineering*, **126**(4), 437-444.

Perez, F.J., S. Pessiki, R. Sause, and L.-W. Lu, (2003). "Lateral Load Tests of Unbonded Post-Tensioned Precast Concrete Walls," *Large-Scale Structural Testing (ACI SP-211)*, 161-182.

Ricles, J.M., R. Sause, M. Garlock, and C. Zhao, (2001). "Post-Tensioned Seismic-Resistant Connections for Steel Frames," *ASCE Journal of Structural Engineering*, **127**(2), 113-121.

Ricles, J.M., R. Sause, S.W. Peng, and L.-W. Lu, (2002). "Experimental Evaluation of Earthquake Resistant Post-Tensioned Steel Connections," *ASCE Journal of Structural Engineering*, **128**(7), 850-859.

Rojas, P., J.M. Ricles, and R. Sause, (2005). "Seismic Performance of Post-Tensioned Steel Moment Resisting Frames with Friction Devices," *ASCE Journal of Structural Engineering*, **131**(4), 529-540.

Sause, R., J.M. Ricles, D. Roke, C.-Y. Seo, and K.-S. Lee, (2006). "Design of Self-Centering Steel Concentrically-Braced Frames," *Proceedings from the 4th International Conference on Earthquake Engineering*, Taipei, Taiwan.

Seo, C.-Y., and R. Sause, (2005a). Influence of Ground Motion Characteristics and Structural Parameters on Seismic Responses of SDOF Systems, *Ph.D. Thesis*, Lehigh University, Bethlehem, PA.

Seo, C.-Y., and R. Sause, (2005b). "Ductility Demands on Self-Centering Systems Under Earthquake Loading," *ACI Structural Journal*, 102(2), 275-285.